SANDIA REPORT
SAND2007-6778J
Unlimited Release
Printed xxxxxxx

Soluble Polytantalate Clusters

May Nyman and Travis M. Anderson

Prepared by
Sandia National Laboratories
Albuquerque, New Mexico 87185 and Livermore, California 94550

Sandia is a multiprogram laboratory operated by Sandia Corporation,
a Lockheed Martin Company, for the United States Department of Energy's
National Nuclear Security Administration under Contract DE-AC04-94AL85000.

Issued by Sandia National Laboratories, operated for the United States Department of Energy by Sandia Corporation.

Available to DOE and DOE contractors from

U.S. Department of Energy
Office of Scientific and Technical Information
P.O. Box 62
Oak Ridge, TN 37831

Telephone: (865) 576-8401
Facsimile: (865) 576-5728
E-Mail: reports@adonis.osti.gov
Online ordering: http://www.osti.gov/bridge

Available to the public from

U.S. Department of Commerce
National Technical Information Service
5285 Port Royal Rd.
Springfield, VA 22161

Telephone: (800) 553-6847
Facsimile: (703) 605-6900
E-Mail: orders@ntis.fedworld.gov
Online order: http://www.ntis.gov/help/ordermethods.asp?loc=7-4-0#online

SAND2007-6778J
Unlimited Release
Printed xxxxxxxx

Soluble Polytantalate Clusters

May Nyman and Travis M. Anderson

Geochemistry Department
Sandia National Laboratories
P.O. Box 5800
Albuquerque, NM 87185-0754
Phone: (505) 284-4484
Fax: (505) 844-7354
Email: mdnyman@sandia.gov

Abstract

Tantalate materials play a vital role in our high technology society: tantalum capacitors are found in virtually every cell phone. Furthermore, electronic characteristics and the incredibly inert nature of tantalates renders them ideal for applications such as biomedical implants, nuclear waste forms, ferroelectrics, piezoelectrics, photocatalysts and optical coatings. The inert and insoluble nature of tantalates is not fundamentally understood; and furthermore poor solubility renders fabrication of novel or optimized tantalates very difficult. We have developed a soft chemical route to water-soluble tantalum oxide clusters that can serve as both precursors for novel tantalate materials and ideal models for experimental and computational approaches to understanding the unusually inert behavior of tantalates. The water soluble cluster, $[Ta_6O_{19}]^{8-}$ is small, highly symmetric, and contains the representative oxygen types of a metal oxide surface, and thus ideally mimics a complex tantalate surface in a simplistic form that can be studied unambiguously. Furthermore; in aqueous solution, these highly charged and super-basic clusters orchestrate surprising acid-base behavior that most likely plays an important role in the inertness of related oxide surfaces. Our unique synthetic approach to the $[Ta_6O_{19}]^{8-}$ cluster allowed for unprecedented enrichment with isotopic labels (^{17}O), enabling detailed kinetic and mechanistic studies of the behavior of cluster oxygens, as well as their acid-base behavior. This SAND report is a collection of two publications that resulted from these efforts.

ACKNOWLEDGMENTS

Sandia is a multiprogram laboratory operated by Sandia Corporation, a Lockheed Martin Company, for the United States Department of Energy's National Nuclear Security Administration under contract DE-AC04-94AL85000. This work was predominantly supported by Sandia National Laboratories' LDRD program, project #113230. It was also supported in part by the National Science Foundation via Grant EAR 05015600 and from the U.S. Department of Energy Office (DOE) of Basic Energy Science via Grants DE-FG03-96ER 14629 and DE-FG03-02ER15693.

TABLE OF CONTENTS

1. Rates of Oxygen-Isotope Exchange Between Sites in the $[H_xTa_6O_{19}]^{8-x}_{(aq)}$ Lindqvist Ion and Aqueous Solutions-Comparisons to $[H_xNb_6O_{19}]^{8-x}_{(aq)}$

Performers: Edina Balogh, Travis M. Anderson, James R. Rustad, May Nyman and William H. Casey

Abstract

Rates of steady oxygen-isotope exchange differ in interesting ways for two sets of structural oxygens in the $[H_xTa_6O_{19}]^{(8-x)-}_{(aq)}$ Lindqvist ion when compared to published data on the $[H_xNb_6O_{19}]^{8-x}_{(aq)}$ version. Because of the lanthanide contraction, the $[H_xTa_6O_{19}]^{(8-x)-}_{(aq)}$ and $[H_xNb_6O_{19}]^{8-x}_{(aq)}$ ions are virtually isostructural and differ primarily in a full core (Kr versus Xe) and the $4f^{14}$ electrons in the $[H_xTa_6O_{19}]^{(8-x)-}_{(aq)}$ ion. For both molecules, both pH-dependent and pH-independent pathways are evident in isotopic exchange of the twelve μ_2-O(H) and six η=O sites. Rate parameters for η=O exchange at conditions where there is no pH-dependence are, for the Ta(V) and Nb(V) versions, respectively, k_0^{298}= $2.72\cdot10^{-5}$ s^{-1} and $9.7\cdot10^{-6}$ s^{-1}, $\Delta H^{\ddagger}$ = 83.6 ± 3.2 and 89.4 kJ·mol^{-1}, and $\Delta S^{\ddagger}$ = -51.0 ± 10.6 and -42.9 J·mol^{-1}·K. For the μ_2-O sites, k_0^{298} =$1.23\cdot10^{-6}$ s^{-1}, $\Delta H^{\ddagger}$ = 70.3 ±9.7 and 88.0 kJ·mol^{-1}, and $\Delta S^{\ddagger}$ = -116.1± 32.7 and -29.4 J·mol^{-1}·K^{-1}. Protonation of the six η=O is energetically unfavored relative to the twelve μ_2-O bridges in both molecules, although not equally so. Experimentally, protonation labilizes both the μ_2-O(H) and η=O sites to isotopic exchange in both molecules. Density-functional electronic-structure calculations indicate that proton affinities of structural oxygens in the two molecules differ with the $[H_xTa_6O_{19}]^{(8-x)-}_{(aq)}$ anion having a smaller affinity to protonate than the $[H_xNb_6O_{19}]^{8-x}_{(aq)}$ ion. This difference in proton affinities is evident in the solution chemistry as pK_a= 11.5 for the $[HTa_6O_{19}]^{7-}_{(aq)}$ and pK_a= 13.6 for the $[HNb_6O_{19}]^{7-}_{(aq)}$ ion. Most striking is the observation that η=O sites isotopically equilibrate faster than the μ_2-O sites for the $[H_xTa_6O_{19}]^{(8-x)-}_{(aq)}$ Lindqvist ion, but slower for the $[H_xNb_6O_{19}]^{8-x}_{(aq)}$ ion, indicating that predictions about site reactivities in complicated structures, such as the interface of aqueous solutions and oxide solids, should be approached with great caution.

Introduction

The early transition metals in their high oxidation states form multimeric metal-oxide clusters, called polyoxometalates, in aqueous solutions. These structures are enormously useful for a myriad of processes in inorganic chemistry, material science, medicine and environmental chemistry.[5-9] Although there is much research on these polyoxometalates, relatively little is known about the pathways by which they react and transform in an aqueous solution[10] yet this information would not only be useful to polyoxometalate researchers, but would also be extraordinarily helpful to scientists trying to understand how larger extended oxide materials such as catalyst supports and clays react in water. Because the polyoxometalate molecules are nanometer in scale and absolutely discrete in size and geometry, experimental data on steady oxygen-isotope-exchange reactions could be easily complemented with DFT or molecular-dynamics simulations to provide real insight into elementary, or near-elementary, reaction pathways[11] and recently for the Nb(V) Lindqvist ion.[4]

The Lindqvist ions comprise one of the simplest classes of polyoxometalates **[Figure 1]** as they consist of a superoctahedron of six $M(O)_6$ octahedra that are linked by twelve μ_2-O(H) bridges at a μ_6-O; each of the six metals is terminated by a η=O. The Lindqvist ion has an internal structural oxygen (μ_6-O) that is inert to exchange[1, 4, 12-17] and the constant ^{17}O-NMR signal from this μ_6-O indicates that the ion remains intact in solution as the other structural oxygens isotopically equilibrate with bulk water. Using this method, in earlier work we studied isotope exchange in the $[HNb_6O_{19}]^{7-}$ Lindqvist ion[4] and found that, at pH~11.5-14, the twelve μ_2-O(H) bridges exchange about ~10 times faster then the η=O sites but, at lower or higher pH values, these two oxygen sites can react at identical rates.[1, 12-17]

In this paper we expand this work and report the rates of isotopic equilibration of the Ta(V) version of this Lindqvist ion. Because of the lanthanide contraction, the Ta(V) and Nb(V) versions of the Lindqvist ions are nearly isostructural. Metals in the two structures have a closed-shell electronic configuration (Xe and Kr, respectively) and primarily differ by the full shell of $4f^{14}$ electrons in the Ta(V) version of the Lindqvist ion. Nevertheless, we show that these molecules react profoundly differently with an aqueous solution in ways that challenge and enrich our understanding of reaction pathways in aqueous solutions.

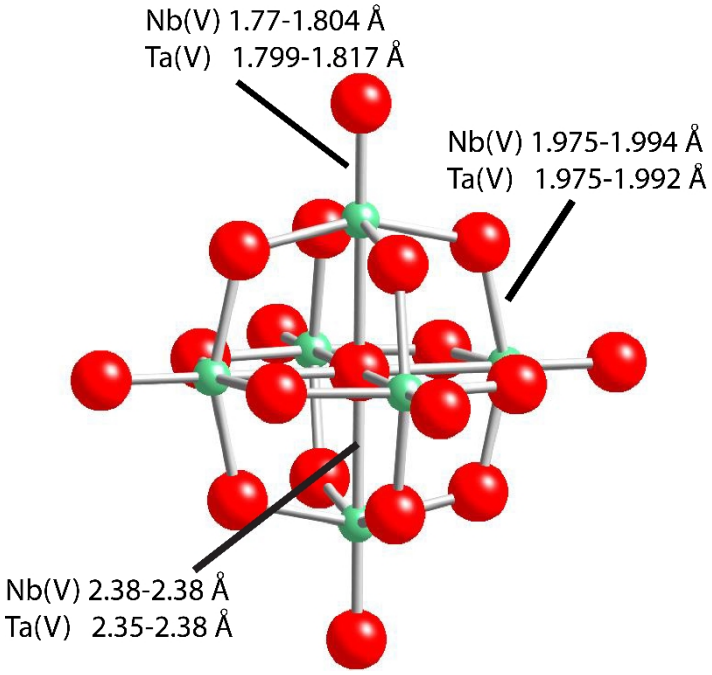

Figure 1. The Lindqvist ions has a central μ_6-O sites that is inert to exchange, twelve μ_2-O bridges and six terminal η=O sites. In the ball-and-stick representation, the oxygens are red and the metals (either Ta(V) or Nb(V)) are green. The bond lengths were determined from X-ray structures of the alkali-metal salts of the Nb(V) and Ta(V) Lindqvist ions in various stoichiometries.[1,3] (Table S-4).

Experimental Methods

Synthesis of the ^{17}O-enriched $[Ta_6O_{19}]^{8-}$ Starting Material

The $NaK_7[Ta_6O_{19}]\bullet 14H_2O$ salt was made by catalyzed decomposition of the $K_3Ta(O_2)_4$ in a basic solution that also contains ^{17}O-enriched water. The resulting solution was slowly evaporated in the presence of KOH to yield crystals of ^{17}O-enriched salts. Most experiments were conducted from a single 2.76 g batch of $NaK_7[Ta_6{}^{17}O_{19}]\bullet 14H_2O$ salt. For this particular synthesis, a 2.00 g (4.7 mmol) sample of K_3TaO_8, 3.83 g (68 mmol) KOH, and 0.137 g (0.6 mmol) of K_3VO_4 were added to 10 mL of water (20% ^{17}O) and the mixture was refluxed and stirred until a clear solution was obtained (~30–45 min). The warm solution was filtered with a 0.45 μm syringe, and 2.76 g of crystalline material was obtained by slow evaporation of the solution at room temperature over two days (91% yield). The ^{17}O-NMR spectrum of the sample indicates a ratio of peak intensities for the μ_6-O, η=O and μ_2-O sites of 1:6:12, as is expected from the molecule's stoichiometry.

Rate Measurements

An experiment was typically begun by dissolving a few tens of milligrams of the $NaK_7[Ta_6{}^{17}O_{19}]\bullet 14H_2O$ salt into an aliquot of isotopically normal background electrolyte solution. At 25 °C, the pH of the resulting self-buffered solution was about 11.5, which is significantly lower than the pH of a corresponding solution made from the $[Nb_6O_{19}]^{8-}$ anion,

which was typically at pH~12.4.[4] Other pH conditions were reached by adding either small amount of 3M KOH to raise pH, or small amounts of K_2CO_3 or $KHCO_3$ to lower pH. These buffers were found previously to have no or little interaction with the Nb(V) Lindqvist ion, which of course is anionic.[4] The ionic strength was maintained nearly constant at 3 M with KCl. The pH-adjusted solutions were typically prepared ahead of time and the salt dissolved into them at temperature.

The pH of each sample was measured on a concentration scale using a glass combination electrode. The electrode was calibrated by Gran titration using 3 M KCl solution and 0.1 M standardized acid at the corresponding temperature. The measured values agree well with those calculated using the concentration of the excess hydroxide ion.

NMR spectroscopy

Variable temperature ^{17}O-NMR measurements were carried out using 10-mm broadband probe on an 11.7 T magnet (ν_o=67.8 MHz for ^{17}O) Bruker Avance spectrometer located at the UCD NMR facility. The spectra were taken with single-pulse excitation using 20 μs s pulses ($\pi/2\approx40$ μ*s*) and recycle delays of 6 ms. The number of acquisition typically varied between 1,000-10,000 with the sample concentration to obtain adequate signal-to-noise ratio. The time-domain data were digitized at 100 kHz. In order to prevent corrosion of the glass, we used a Teflon insert fitted into the 10-mm NMR tubes. Although this insert prevented corrosion of the glass, it did allow CO_2 to enter the solutions, which was detectable as a slow pH drift in the long-term experiments. The temperature was measured by replacing the sample with a solution of background electrolyte containing a copper-constantan thermocouple fitted into the NMR tube. The accuracy of the measured temperature was about ±0.1 K.

DFT Calculations

The calculations were conducted using both the conductor-like screening model (COSMO[18]) or by terminating the structures with potassium in order to reduce the anionic charge and maintain electronic stability.[19] All calculations were conducted using the PQS code from Parallel Quantum Solutions, Inc. (http://www.pqs-chem.com). The B3LYP exchange-correlation functional was used, as implemented in the PQS code. The LANL2DZ basis set was chosen for the Nb(V) and Ta(V) metals. This basis set employs an effective core potential which partially takes into account relativistic effects. The basis set 6-31G* was chosen for the oxygens, potassiums and hydrogens.

Results

The ^{17}O NMR spectrum of the hexatantalate solution contains four conspicuous peaks that are assignable to the η=O (470-490 ppm), μ_2-O(H) (320-330 ppm), μ_6-O (near -40 ppm) and bulk water peak at 0 ppm **[Figure 2-top]**. At the earliest spectrum (t_0 is typically 4-7 minutes after dissolution of the salt), the integrated areas of the peaks has nearly the ratio of 6:12:1, corresponding to the six equivalent η=O, the twelve μ_2-O(H) and the single μ_6-O site. These peak assignments agree with previous ^{17}O NMR spectra of the Ta(V) Lindqvist ions.[14, 20]

The ^{17}O NMR peak positions vary with pH, but not with temperature in the range we investigated (5.2 – 48.8 °C), suggesting that protonation equilibrium affects the peak positions. This variation with pH is important because the acid-base equilibrium constants for the $[H_xTa_6O_{19}]^{(8-x)-}$ ion are poorly known, as are protonation equilibrium constants for Lindqvist ions in general. Because the molecules are so basic, protonation constants cannot be reliably determined by pH potentiometric titration. The cluster dissociates below pH=10 and forms a precipitate that limits the pH range that can be investigated. The absorbance of the $[H_xTa_6O_{19}]^{(8-x)-}$ ion overlaps with the absorbance of the background electrolyte so that UV-Vis spectrophotometry is equivocal.

However, the protonation of different oxygen sites on the $[H_xTa_6O_{19}]^{(8-x)-}$ ion apparently leads to a deshielding of peaks **[Figure 3]** that can allow us to estimate conditional protonation constants. The peak positions, $\delta_{obs,}$ can be expressed as in

$$\delta_{i,\,obs} = \sum_{n=1}^{N} \delta_{i,\,H_nL} \times f_{H_nL} \qquad (1)$$

where δ is the intrinsic chemical shift of the *i* nucleus of the H_nL species (ppm) and f_{HnL} is the fractional population of each species. For this calculation, the bulk water peak was set δ = 0. The protonation constants, K_a, are then related to the f_{HnL} by:

$$K_a = \frac{f_{H_nL}}{f_{H_{n-1}L}\left[H^+\right]} \qquad (2)$$

and optimized via nonlinear least-squares fitting algorithm to yield pK_{a1}= 9.3 and pK_{a2} = 11.5 as the most likely values. The pH range investigated was too small to reliably assign uncertainties to these pK_a values, but they allow us to make reasonable estimates of the fraction of various protonated forms of the $[H_xTa_6O_{19}]^{(8-x)-}$ ion as a function of pH **[Figure 4]**. The pK_a values for the $[H_xTa_6O_{19}]^{(8-x)-}$ ion are somewhat lower than those reported for the $[H_xNb_6O_{19}]^{(8-x)-}$ (pK_{a1}=9.35, pK_{a2}=9.92, pK_{a3}=13.63) [2, 21].

Calculated Proton Affinities of the Ta(V) and Nb(V) Lindqvist Ions

As discussed above, the two molecules differ subtly in their solution chemistry as the $[Ta_6O_{19}]^{8-}$ Lindqvist ion is somewhat less basic than the corresponding $[Nb_6O_{19}]^{8-}$ cluster. This difference in acid-base chemistry is manifested in the estimated pK_a values as well as in the results of density-functional (DFT) calculations.

The DFT calculations indicate clear differences between the two molecules that are consistent with experiment. It has been shown that electronic energies of isostructural molecules calculated at 0 K are a good indicator of solution pK_a.[22, 23] The bridging oxo sites have a higher affinity for protons relative to the terminal Nb(η=O) and Ta(η=O) sites, as is common for polyoxometalates where terminal oxygens have higher bond orders than bridging oxygens. Thus, the experimental structures of Ozeki et al.,[24] and Nyman et al.,[1] show that the protons bond to the bridging oxygens in the niobate cluster. In the solid state, the $[Ta_6O_{19}]^{8-}$ anion has never been crystallized, which is consistent with our observation that the Nb(V) ion is more basic than the Ta(V) Lindqvist ion. All solid-state structures of $[Ta_6O_{19}]$ salts are of the non-protonated form.[3, 25-27]

Almost independent of the position of protonation, a given oxygen in the Nb(V) Lindqvist ion has a consistently higher affinity for protons than the corresponding Ta(V) structure. For example, the energies for proton transfer from a bridging oxygen:

$$[Nb_6O_{19}]^{8-} + [Ta_6(\mu_2\text{-}OH)O_{18}]^{7-} = [Ta_6O_{19}]^{8-} + [Nb_6(\mu_2\text{-}OH)O_{18}]^{7-}$$

and

$$K_8Nb_6O_{19} + K_7Ta_6(\mu_2\text{-}OH)O_{18} = K_8Ta_6O_{19} + K_7Nb_6(\mu_2\text{-}OH)O_{18}$$

are -34 and -23 $kJ\cdot mol^{-1}$, respectively, consistent with bridging oxygens on the Nb(V) Lindqvist ion having a higher proton affinity than the corresponding Ta(V) ion. Similar results are achieved regardless of the initial protonation states of the Nb(V) and Ta(V) structures and whether a potassium-terminated cluster or the COSMO solvent model is employed to achieve electronic stability. The one exception is proton transfer between the two η=O:

$$K_8Nb_6O_{19} + K_7Ta_6(\eta\text{-}OH)O_{18} = K_8Ta_6O_{19} + K_7Nb_6(\mu\text{-}OH)O_{18}$$

which has a negligible energy difference.

Because the Nb(V) and Ta(V) molecules have equal preference for a proton at a η=O, differences among μ_2-O account for the overall differences in proton affinities between the two molecules. Thus, energies for reactions: $[Nb_6(\eta_2\text{-}OH)O_{18}]^{7-} = [Nb_6(\mu_2\text{-}OH)O_{18}]^{7-}$ and $[Ta_6(\eta_2\text{-}OH)O_{18}]^{7-} = [Ta_6(\mu_2\text{-}OH)O_{18}]^{7-}$ are -60 and -45 kJ mol^{-1}, respectively. Corresponding energies for the potassium-terminated structures in the gas phase: $[K_7Nb_6(\eta_2\text{-}OH)O_{18}] = [K_7Nb_6(\mu_2\text{-}OH)O_{18}]$ and $[K_7Ta_6(\eta_2\text{-}OH)O_{18}] = [K_7Ta_6(\mu_2\text{-}OH)O_{18}]$ are -37 and -15 kJ mol^{-1}. In other words, the energy to move a proton from a bridge to a terminal oxo is always unfavorable, but is considerably less unfavorable for the tantalate than for the niobate. Protons lifetimes are undoubtedly less than, or equal to 10^{-3} seconds on these molecules[28], which means that the proton will visit all oxygens during the timescale of oxygen-isotope exchange in either molecule, although not to equal extents. As we discuss below, an important experimental observation is that protonation by 2-3 protons apparently labilizes both η=O and μ_2-O(H) in the clusters, which is surprising.

Oxygen-Isotope Exchange Rates

The rates of oxygen-isotope exchange between bulk water and the isotopically enriched $[H_xTa_6O_{19}]^{(8-x)-}$ ion were estimated from diminution of the ^{17}O NMR signal from the η=O and μ_2-O(H) sites as a function of time. During these experiments, the peaks corresponding to the μ_6-O exhibited no appreciable change in intensity, indicating that the molecule remains intact as the isotope-exchange reactions proceed at the other sites **[Figures 2, 5]**. A typical exponential decay of the peak intensity as a function of time is shown in **Figure 5**, along with a fit to the data. The pseudo-first-order rate constants (k_{obs}) were calculated by fitting the intensity data to:

$$I_t = (I_0 - I_e)\exp(-k_{obs}t) + I_e \qquad (3)$$

where I_t, I_0 and I_e are the intensity values at time t, zero and equilibrium, respectively, and time was measured in seconds. The results of the experiments are shown in **Figure 6**, where they are compared with similar data for the Nb(V) version of the molecule.[4]

There are several important features of the rate data for the $[H_xTa_6O_{19}]^{(8-x)-}$ molecule when compared with $[H_xNb_6O_{19}]^{(8-x)-}$ ion. First, the overall reactivities of the two molecules are broadly similar. Secondly, the relative reactivities of the η=O and μ_2-O(H) sites in the $[H_xTa_6O_{19}]^{(8-x)-}$ are opposite in the $[H_xNb_6O_{19}]^{(8-x)-}$ ion. For the $[H_xNb_6O_{19}]^{(8-x)-}$ ion in the pH range 12.5<pH<14.5, the rates of isotopic exchange of the η=O and μ_2-O(H) sites differ by about a factor of ten from one another and the η=O sites react more slowly than the μ_2-O(H) sites **[Figure 6].** For the $[H_xTa_6O_{19}]^{(8-x)-}$ ion in the same pH region, the η=O site reacts about a factor of ten more rapidly than the μ_2-O(H) sites.

Thirdly, the pH-dependencies of the rates for both the η=O and the μ_2-O(H) sites are distinctly different from one another in the Ta(V) and Nb(V) versions of the molecules. Although for both molecules, the rates in the pH region of 12.5<pH<14.5 are largely independent of pH. An additional difference is that the rates of isotopic exchange for the μ_2-O(H) site in the $[H_xNb_6O_{19}]^{(8-x)-}$ molecule exhibits a slight pH dependence and eventually becomes equivalent in rate to the η=O site at pH~14.5 **[Figure 6]** whereas the rates for the $[H_xTa_6O_{19}]^{(8-x)-}$ molecule remain separate from one another at all conditions.

A profound pH dependence in the reaction rates, affecting both the η=O and the μ_2-O(H) sites, becomes evident at pH<11.5 for the $[H_xTa_6O_{19}]^{(8-x)-}$ ion and pH<12 for the $[H_xNb_6O_{19}]^{(8-x)-}$ ion. For the $[H_xNb_6O_{19}]^{(8-x)-}$ ion, the rates of isotopic exchange of the η=O and the μ_2-O(H) sites converge as pH drops. For the $[H_xTa_6O_{19}]^{(8-x)-}$ ion, the rates of isotopic exchange of the η=O and the μ_2-O(H) sites never converge but continue to differ by roughly an order of magnitude in rate. It is particularly interesting that both the η=O and the μ_2-O(H) sites are labilized in both molecules as pH drops. Both the structural data and the DFT calculations indicate that protonation of the η=O sites is always unfavored relative to the μ_2-O. Apparently, when a μ_2-O is protonated, the rates of isotopic exchange of all oxygens, except of course the inert μ_6-O, increase.

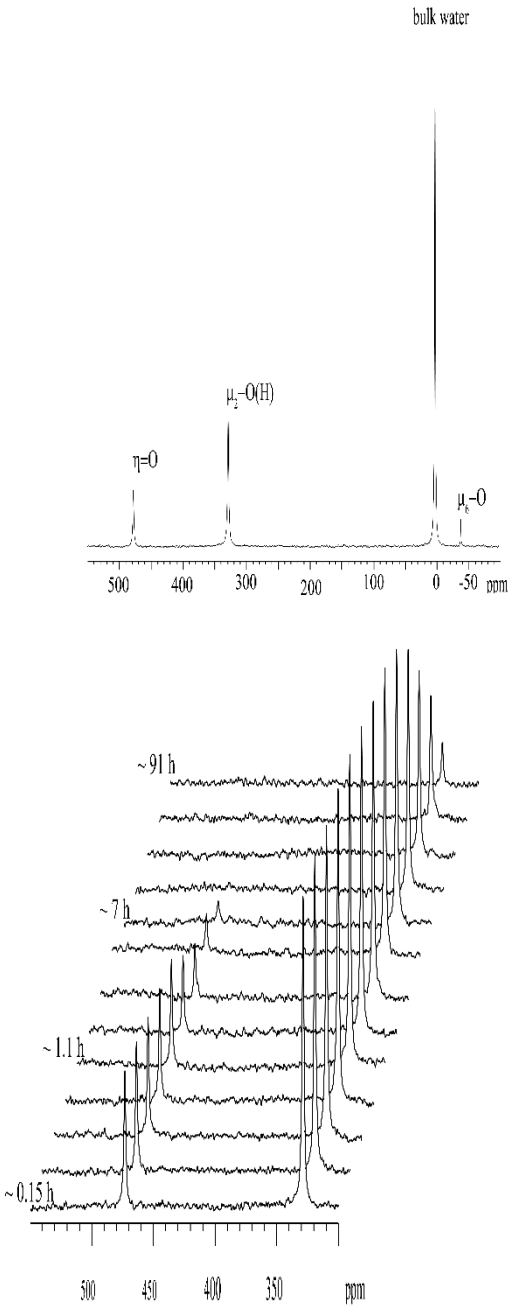

Figure 2: (top) ^{17}O-NMR peaks assigned to the μ_2-O(H) (top, ~320 ppm) and η=O (~470 ppm), the bulk-water peak (0 ppm) and the μ_6-O (~-40 ppm). The intensity ratios μ_2-O(H):η=O:μ_6-O vary 12:6:1, approximately. **(bottom)** Successive specta showing the time variation in peaks assigned to the μ_2-O(H) and η=O at pH~12.8.

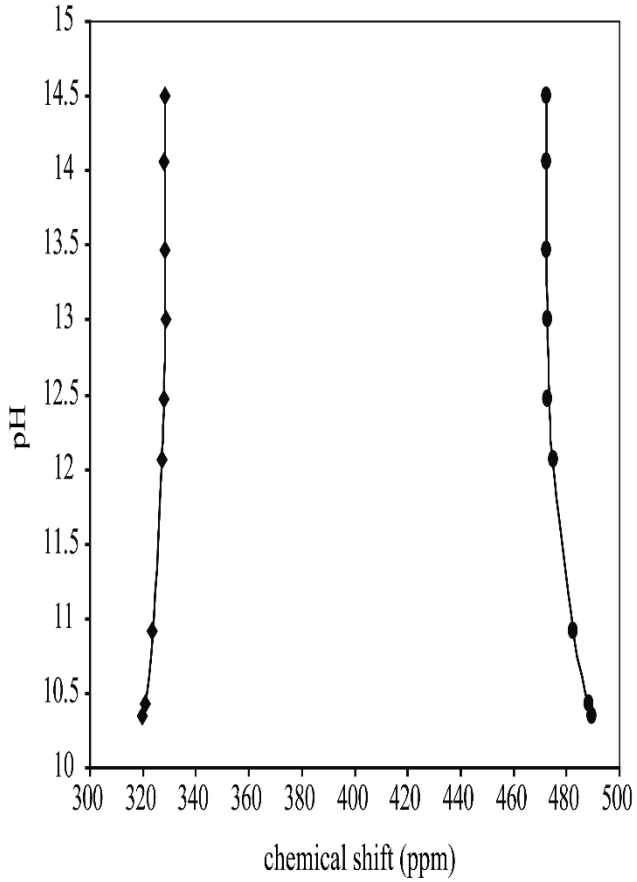

Figure 3: The ^{17}O-NMR peak positions of the η=O (470-490 ppm) and the μ_2-O(H) (320-330 ppm) vary with pH at constant temperature. Lines are fits of Eqn. (2) to the data, yielding pK_{a1}= 9.3 and pK_{a2} = 11.5 for the $[H_xTa_6O_{19}]^{(8-x)-}$ ion.

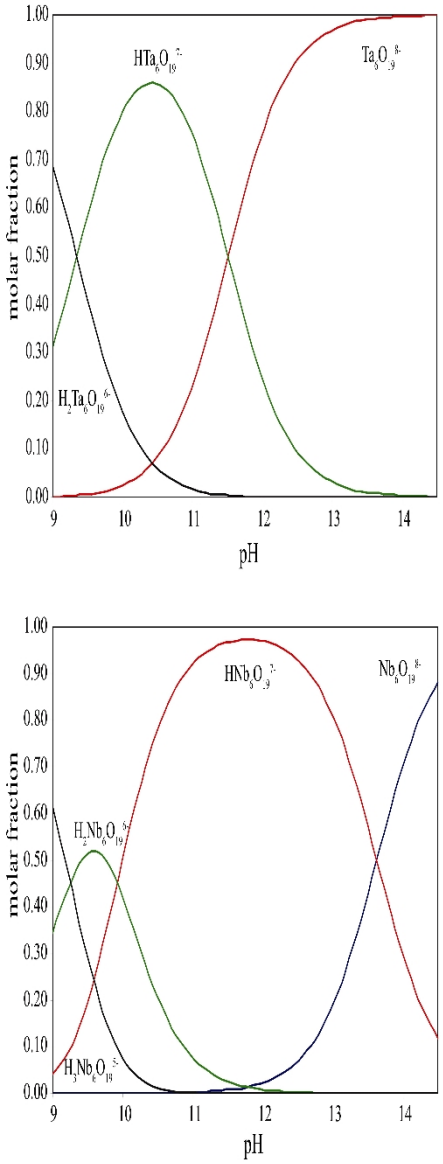

Figure 4: Speciation diagram showing the various forms of $[H_xTa_6O_{19}]^{(8-x)-}$ ion (x=0, 1, 2) (top) $[H_xNb_6O_{19}]^{(8-x)-}$ ion (x=0, 1, 2, 3) (bottom) in aqueous solution as a function of pH at I=3.0 M. The values of the pK_a are determined by least-squares fit to ^{17}O-NMR data **[Figure 3]**. The plot for $[H_xNb_6O_{19}]^{(8-x)-}$ employed data from previous work.[2]

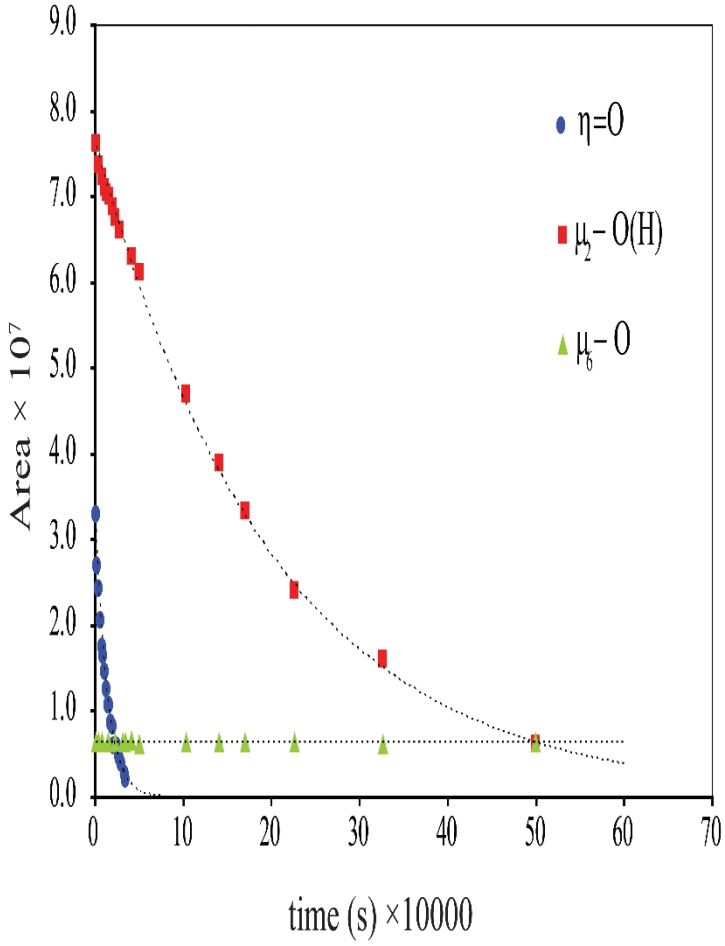

Figure 5: The intensity of ^{17}O signal in a given peak decreases exponentially with time. Here the intensity of the η=O and μ_2-O peaks decrease exponentially, while the signal for the central μ_6-O is constant, indicating that the molecule remains intact during the reaction. The rate coefficients, $k_{obs,}$ and characteristic time, $\tau=1/k_{obs}$, is determined by a fit of Eqn. (3) to the data. The enriched compound was dissolved in 2 ml of 3M KOH.

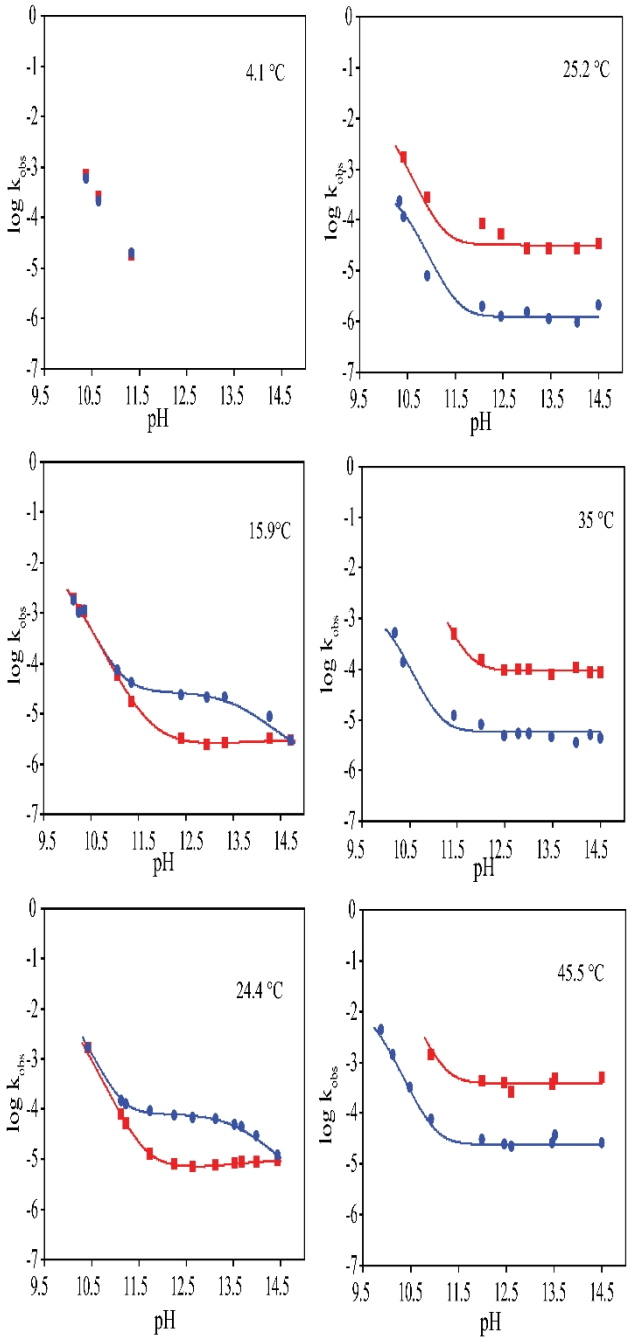

Figure 6: Rates as a function of pH and temperature for the $[H_xNb_6O_{19}]^{(8-x)-}$ (**left**) and $[H_xTa_6O_{19}]^{(8-x)-}$ (**right**) Lindqvist ions. Data for the $[H_xNb_6O_{19}]^{(8-x)-}$ are from reference 4. The data for the μ_2-O(H) are in blue circles and the data for the η=O are in red squares. The lines correspond to fits of a rate law (Eqn. 4) to the data.

Discussion

Rate Law

The results described above indicate that the pathways for oxygen-isotope exchange at η=O and μ_2-O(H) sites in the $[H_xTa_6O_{19}]^{(8-x)-}$ and $[H_xNb_6O_{19}]^{(8-x)-}$ Lindqvist ions are distinct from one another. These differences are striking in light of the considerable structural and electronic similarity between these two structures. Nevertheless, the rate data can be fit to the same general rate law that described the Nb(V) version of the molecule. Black et al.[4] used the following equation:

$$k_{obs} = \sum_{i=0}^{2} k_i \cdot X_i .... \qquad (4)$$

where, in this case, k_i indicates the rate constants and X_i is the mole fraction of each protonation stoichiometry (e.g., x=0-2 in $H_xTa_6O_{19}^{(8-x)-}$). The mole fractions are given by:

$$X_0 = \frac{[Ta_6O_{19}^{8-}]}{\Sigma[H_xTa_6O_{19}^{(8-x)-}]} \quad X_1 = \frac{[HTa_6O_{19}^{7-}]}{\Sigma[H_xTa_6O_{19}^{(8-x)-}]} \quad X_2 = \frac{[H_2Ta_6O_{19}^{6-}]}{\Sigma[H_xTa_6O_{19}^{(8-x)-}]}$$

where the subscripts refer to the number of protons on the $[H_xTa_6O_{19}]^{(8-x)-}$ ion. These mole fractions can be calculated from conditional equilibrium constants:

$$x_{Ta_6O_{19}^{8-}} = \frac{K_{a1} \cdot K_{a2}}{[H^+]^2 + [H^+] \cdot K_{a1} + K_{a1} \cdot K_{a2}}$$

$$x_{HTa_6O_{19}^{7-}} = \frac{K_{a1} \cdot [H^+]}{[H^+]^2 + [H^+] \cdot K_{a1} + K_{a1} \cdot K_{a2}}$$

$$x_{H_2Ta_6O_{19}^{6-}} = \frac{[H^+]^2}{[H^+]^2 + [H^+] \cdot K_{a1} + K_{a1} \cdot K_{a2}}$$

This rate law implies that the various protonated forms of the molecule contribute independently to the overall rate, and that the incoming moiety is probably a water molecule and not a hydroxide or hydronium ion. Although this explanation is simple, we evaluated other models as well, including cases where the pK_a values were allowed to vary as adjustable parameters, where different protonated stoichiometries were considered.

The curve-fitting exercise yielded interesting results. First, inclusion of the $HTa_6O_{19}^{7-}$ stoichiometry had practically no effect on the quality of the resulting fit**.** Therefore, this stoichiometry was apparently not necessary to adequately fit the data. In contrast, excluding the $H_2Ta_6O_{19}^{6-}$ stoichiometry always led to a much poorer fit. These fits, of course, are sensitive to the acid-base chemistry of the molecule, which is constrained only by our ^{17}O-NMR data as there are no independent estimates. We can think of no reasonable explanation for the absence of a monoprotonated species and preference for the diprotonated species, but the most interesting point is that protons at any site apparently labilize both η=O and μ_2-O(H) sites. Nevertheless, we consistently found that varying the pK_a values had little effect on the value of k_0,

corresponding to the $Ta_6O_{19}^{8-}$ stoichiometry, while the higher values of k_2 were highly sensitive to changes in acid-base equilibrium, as one expects. In these fits, the deviation of pK_a from values determined from the NMR titration were in the range of 0.1-1 units. Although adequate fits could be achieved by adding an explicit dependence of rate on $[H_3O^+]$, we excluded this model as unreasonable. At the high pH conditions of these experiments, it is more reasonable to assume that water molecules are the isotopically exchanging moiety, as was concluded for the $H_xNb_6O_{19}^{(8-x)-}$ by Black et al.[4]

At high pH where the $Ta_6O_{19}^{8-}$ stoichiometry dominates, there is no dependence of rate on solution pH. At these conditions, we could examine the temperature dependency of k_{obs} using the Eyring equation:

$$\frac{1}{k_{obs}} = \frac{k_B T}{h} e^{-\left(\frac{\Delta H^{\ddagger} - T\Delta S^{\ddagger}}{RT}\right)} \qquad (5)$$

where k_B is Boltzmann's constants, h is Planck's constant, R is the gas constant and T is the experimental temperature in Kelvin. The activation parameters are reported in Table 1 where they are compared to those of Black et al.,[4] for the $Nb_6O_{19}^{8-}$ molecule at a similar condition. In estimating the activation parameters for the $Ta_6O_{19}^{8-}$ molecule we excluded two values at the lowest temperature because we suspect that the rate estimates were affected by CO_2 uptake and pH drift **[Figure 7]**. All data were included for the terminal peak, which reacted relatively quickly. (Experiments at higher temperatures are only a few dozen hours whereas those at lower temperatures take weeks.) The solutions in these two samples had relatively low buffer capacity and the rate experiments were particularly long, allowing CO_2 to diffuse into the sample tubes.

Pathways for Isotope Exchange

In considering isotope-exchange reactions in the $[H_xNb_6O_{19}]^{(8-x)-}$ ion, Black et al.[4] suggested that one of the three mutually orthogonal $M_4(\mu_2\text{-}O)_4(\eta\text{-}O)_4$ rings opens to become a precursor to isotopic exchange. This pathway was appealing because η=O and μ_2-O(H) sites in the Nb(V) Lindqvist ion sometimes react at equal rates and, in the ring-opened structure, the η=O and μ_2-O(H) become temporarily equivalent. At this point, the Nb(V) metals also become undercoordinated and well exposed to an incoming water molecule that can transfer protons and replace one of the structural oxygens. Black et al.[4] suggested the ring-opened structure might actually be a metastable form of the molecule, by analogy with other polyoxocations.[29]

However, the η=O and μ_2-O(H) rates for the $[H_xTa_6O_{19}]^{(8-x)-}$ ion always differ from one another and there is no need to invoke a mechanism that makes these two oxygens equivalent. Alternative to the large-scale ring-opening mechanism of Black et al.[4], reaction could be at a single metal site, where η=O and μ_2-O(H) within a $Ta_4(\mu_2\text{-}O)_4(\eta\text{-}O)_4$ ring rotate and allow access of the water to the metal. The incoming water molecule can transfer protons to an outgoing structural oxygen, which leaves as a water molecule. The immediate analogy is isotopic exchange of a carbonyl oxygen in an ester.

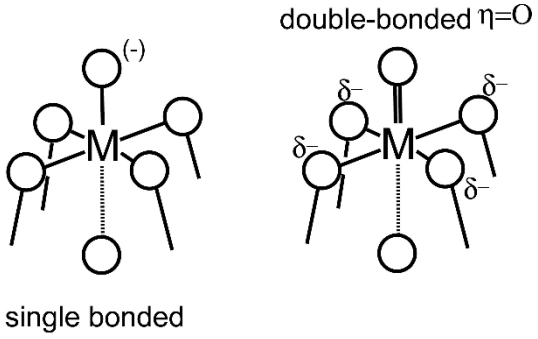

A qualitative explanation for the differences in reactivities of isostructural Nb(V) and Ta(V) Lindqvist ions derives from the original work of Day and Klemperer[13], who invoked two extreme resonance structures to explain the reactivities of η=O and μ_2-O sites. In one structure, the pentavalent charge is distributed across five single bonds (the bond to the central μ_6-O is so long and weak as to be ignored), with the anion charge centered on the η=O. For this structure, the terminal oxygens are expected to be more labile than the bridges, as we observe for the Ta(V) Lindqvist ion. An alternative form is a doubly bonded η=O with bonds to bridging oxygens having bond orders less than unity; 3/4 bond orders would account for the +5 metal charge. In this resonance structure, the terminal oxo is unreactive relative to the bridges, as we observe for the Nb(V) Lindqvist ion.

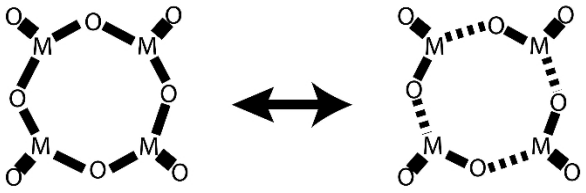

An alternative interpretation was suggested to us by Prof. Craig Hill and invokes alternating differences in bond orders in the $M_4(\mu_2\text{-}O(H))_4(\eta\text{-}O)_4$ rings, by analogy with such quasi-conjugation in tungstates.[30, 31] The essential idea is that the $Nb_4(\mu_2\text{-}O(H))_4(\eta\text{-}O)_4$ rings have a greater extent of alternating bond conjugation than the $Ta_4(\mu_2\text{-}O(H))_4(\eta\text{-}O)_4$ rings. This difference is manifested in a higher proton affinity (to the singly-bonded oxygen in the ring) and the greater lability of one of the bridging oxygens as the ring opens for the niobate, but not the tantalate.

We see no evidence in the electronic-structure calculations for differences in natural bond orders in the mutually orthogonal $M_4(\mu_2\text{-}O)_4(\eta\text{-}O)_4$ rings that might suggest a heterogeneity in bonding to μ_2-O(H) between the tantalate and niobate structures. There are small differences in NBO charges on the oxygens in the $Ta_4(\mu_2\text{-}O)_4(\eta\text{-}O)_4$ and $Nb_4(\mu_2\text{-}O)_4(\eta\text{-}O)_4$ rings, but these differences are inconsistent with the proton affinities and offer no clear suggestion of a pathway. Similarly, we see no evidence for bond conjugation in the $M_4(\mu_2\text{-}O)_4(\eta\text{-}O)_4$ rings and have more extensive simulations underway.

Table 1: Activation parameters for oxygen-isotope exchange for sites in the Ta(V) and Nb(V) versions of the Lindqvist ions.[32]

	pH	η=O		μ_2-O	
		$\Delta H^{\neq}$ (kJ mol^{-1})	$\Delta S^{\neq}$ (J K^{-1} mol^{-1})	$\Delta H^{\neq}$ (kJ mol^{-1})	$\Delta S^{\neq}$ (J K^{-1} mol^{-1})
Ta(V)	13	83.6 ± 3.2	-51.0 ± 10.6	70.3 ± 9.7	-116.1 ± 32.7
Nb(V)	~13	89.4	-42.9	88.0	-29.7

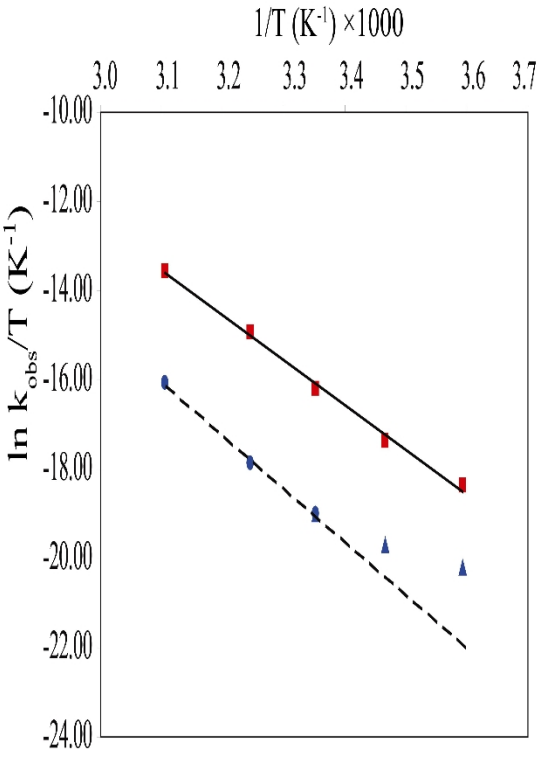

Figure 7: The temperature dependence of k_{obs} for the μ_2-O (blue) and η=O (red). The solid and dashed lines, respectively, correspond to fits of Eqn. (5) to the data. The lowest-temperature points for the η=O were excluded because these experiments were quite lengthy and we suspect that the rate estimates were affected by pH-drift.

Conclusions

Oxygen-isotope-exchange rates were measured on the Ta(V) Lindqvist ions as a function of pH and temperature and these new data allow a useful comparison with the isostructural Nb(V) version. We find tantalizing differences in reactivities. First, the η=O oxygens in the Ta(V) molecule react faster than the μ_2-O(H), which is opposite to what is observed in the Nb(V) version molecule where the μ_2-O(H) reacts faster than the η=O oxygens in the pH range ~12<pH<14.5. Secondly, unlike in the $H_xNb_6O_{19}^{(8-x)-}$ molecule, the μ_2-O(H) and η=O oxygens in the $H_xTa_6O_{19}^{(8-x)-}$ molecule never react at the same rates. Thirdly, the activation parameters for the $H_xNb_6O_{19}^{(8-x)-}$ and $H_xTa_6O_{19}^{(8-x)-}$ suggest that the oxygen sites react via different pathways, in spite of the similarities of these molecules in electronic and physical structure. High pressure NMR could be a useful tool to confirm these proposed differences in reaction mechanisms.

In both molecules, rates at both the η=O and μ_2-O(H) increase as the molecules become protonated, which are probably at the bridging oxygens. This general labilization may be extraordinarily important for understanding reactions at extended oxide surfaces. Protonation of the μ_2-O is energetically favored by a few tens of kJ mol^{-1} relative to the η=O, but not equally so. The energy difference associated with moving a proton from a μ_2-OH to the η=O on the $H_xTa_6O_{19}^{(8-x)-}$ molecule is less than for the $H_xNb_6O_{19}^{(8-x)-}$ by ~15 kJ mol^{-1}, suggesting that protonation of the η=O may be more involved in labilizing the molecule than for the $H_xNb_6O_{19}^{(8-x)-}$ ion. In general, proton affinities of oxygens on the $H_xNb_6O_{19}^{(8-x)-}$ are greater than for the corresponding site on the $H_xTa_6O_{19}^{(8-x)-}$, which is also evident in the experimental data.

These Lindqvist ions present interesting challenges to computation chemistry, as the comparison is so direct and fair. The fact that the oxygen sites react so unpredictably between these molecules suggests that models for site reactions at extended structures, for which data are more difficult to acquire, should be approached with caution. Our experience with aluminum polyoxocations[11] indicates that little can be understood definitively about the reaction pathways in a class of clusters until data are available for several compositions. Thus we have experiments underway to synthesize and study the isotope exchange reactions other Lindqvist ions including $[W_4Nb_2O_{19}]^{4-}$).

References

1 M. Nyman, T. M. Alam, F. Bonhomme, M. A. Rodriquez, C. S. Frazer, M. E. Welk, *J. Clust. Sci.* 2006, **17**, 197.

2 N. Etxebarria, L. A. Fernandez, J. M. Madariaga, *Chem. So., Dalton Trans.* 1994, **20**, 3055.

3 T. M. Anderson, T. M. Alam, F. Bonhomme, M. A. Rodriguez, M. Nyman, *Dalton Trans.* 2007, in press.

4 J. R. Black, M. Nyman, W. H. Casey, *J.Am. Chem. Soc.* 2006, **128**, 45, 14712.

5 C. L. Hill, *J. Mol. Catal. A: Chem.* 2007**, 262**, 2.

6 D.-L. Long, E. Burkholder, L. Cronin, *Chem. Soc. Rev.* 2007, **36**, 105.

7 D. E. Katsoulis, *Chem. Rev.* 1998, **98**, 359.

8 J. T. Rhule, C. L. Hill, D. A. Judd, R. F. Schinazi, *Chem. Rev.* 1998, **98**, 327.

9 A. Müller, F. Peters, M. T. Pope, *Chem. Rev.* 1998, **98**, 239.

10 C. L. Hill, *Comp. Coord. Chem. II* 2004, **4**, 679.

11 W. H. Casey, *Chem. Rev.* 2006, **106**, 1.

12 T. M. Alam, M. Nyman, B. R. Cherry, J. M. Segall, L. E. Lybarger, *J. Am. Chem. Soc.* 2004**, 126**, 5610.

13 V. W. Day, W. G. Klemperer, *Science* 1985, **228**, 533.

14. A. D. English, J. P. Jesson, W. G. Klemperer, T. Mamouneas, L. Messerle, W. Shum, A. Tramontano, *J. Am. Chem. Soc.* 1975, **97**, 4785.
15. M. Filowitz, R. K. C. Ho, W. G. Klemperer, W. Shum, *Inorg. Chem.* 1979, **18**, 93.
16. W. G. Klemperer, in *Inorganic Syntheses* 1990, **27**, 71.
17. W. G. Klemperer, in *NATO ASI Series, Series C: Mathematical and Physical Sciences* 1983, **103**, (Multinucl. Approach NMR Spectrosc.), 245.
18. A. Klamt, V. Jonas, T. Buerger, J. C. W. Lohrenz, *J. Phys. Chem. A* 1998, **102**, 5074.
19. X. Lopez, J. A. Fernandez, S. Romo, J. F. Paul, L. Kazansky, J. M. Poblet, *J. Comp. Chem.* 2004, **25,** 1542.
20. C. J. Besecker, W. G. Klemperer, D. J. Maltbie, D. A. Wright, *Inorg. Chem.* 1985, **24**, 1027.
21. G. M. Rozantsev, O. I. Dotsenko, G. V. Taradina, *Koord. Khim.* 2000, **26**, 247.
22. J. R. Rustad, D. A. Dixon, J. D. Kubicki, A. R. Felmy, *J. Phys. Chem. A* 2000, **104**, 4051.
23. J. R. Rustad, D. A. Dixon, K. M. Rosso, A. R. Felmy, *J. Am. Chem. Soc.* 1999, **121**, 3234.
24. T. Ozeki, T.Yamase, H. Naruke, Y. Sasaki, *Bull. Chem. Soc. Jpn.* 1994, **67**, 3249.
25. H. Hartl, F. Pickhard, F. Emmerling, C. Roehr, *Z. Anorg. Allg. Chem.* 2001, **627**, 2630.
26. I. Lindqvist, B. Aronsson, *Ark. Kemi* 1953, **6**, 49.
27. F. Pickhard, H. Hartl, *Z. Anorg. Allg. Chem.* 1997, **623**, 1311.
28. J. R. Houston, B. L. Phillips, W. H. Casey, *Geochim. Cosmochim. Acta* 2006, **70**, 1636.
29. J. R. Rustad, J. S. Loring, W. H. Casey, *Geochim. Cosmochim. Acta* 2004, **68**, 3011.
30. N. Leclerc-Laronze, M. Haouas, J. Marrot, F. Taulelle, G. Hervé, *Angew. Chem. Int. Ed.* 2005, **45**, 139.
31. X. Fang, C. L. Hill, *Angew. Chem. Int. Ed.* 2007, **46**, 3877.
32. J. R. Black, M. Nyman, W. H. Casey, *J. Am. Chem. Soc.* 2007, **129**, 5298.

2. An Aqueous Route to $[Ta_6O_{19}]^{8-}$ and Solid-State Studies of Isostructural Niobium and Tantalum Oxide Complexes

Performers: Travis M. Anderson, Mark A. Rodriguez, François Bonhomme, Joel N. Bixler, Todd M. Alam, and May Nyman

Abstract

A new soft chemical route to $[Ta_6O_{19}]^{8-}$ has been developed by the dissolution of $[Ta(O_2)_4]^{3-}$ in conditions alkaline enough to arrest formation of Ta_2O_5, followed by $[VO_4]^{3-}$-catalyzed decomposition of the peroxide ligands and crystallization of the salt. An average of bond lengths and angles from isostructural salts of $[Ta_6O_{19}]^{8-}$ and $[Nb_6O_{19}]^{8-}$ indicate there is an increase in terminal M(η=O) bond lengths and M-μ_2-O-M angles and a decrease in bridging μ_2-O-M bond lengths in $[Ta_6O_{19}]^{8-}$, although the central μ_6-O-M bond lengths are identical within experimental error. Two new structures of $Na_7[HNb_6O_{19}]\bullet 15H_2O$ (**1**) and $Na_8[Ta_6O_{19}]\bullet 15H_2O$ (**2**) are exemplary of the fact that protonated μ_2-OH are observed exclusively in the niobates. In these structures, the metal-oxide framework, seven sodium atoms, and all fifteen water molecules are located in identical unit cell positions, but in **2** an eighth charge-balancing sodium is located in close proximity to the protonated μ_2-OH in **1**. Differences in the basicity of Nb(V)- and Ta(V)-bound oxygen atoms are also manifested at the surfaces of ^{17}O-enriched powders of Nb_2O_5 and Ta_2O_5. Oxygen exchange at the surface of these materials readily takes place at both terminal and bridging sites in Nb_2O_5 but only at terminal sites in Ta_2O_5.

Introduction

There is a prevailing paradigm that tantalum is chemically similar to niobium due to their related electronic configurations and because their pentavalent ions are virtually identical in size as a result of the lanthanide contraction.[1] Both niobium and tantalum form base-soluble pentaoxides and alkali-metal oxides such as perovskite and pyrochlore analogues.[2,3] In addition, the polyoxometalate (POM) chemistry of niobium and tantalum is dominated by the Lindqvist ion ($[M_6O_{19}]^{8-}$, where M = Nb(V) or Ta(V)) which is primarily stable in alkaline aqueous media.[4-8]

The Lindqvist cluster geometry is ideal as a structural and reactivity model for metal oxide surfaces.[7,8] It contains representative interfacial oxygen types, bridging (μ_2-O) and terminal (η=O), that are easily discerned by ^{17}O NMR spectroscopy.[6] Previously, ^{17}O NMR was used to measure oxygen-isotope exchange rates of the μ_2-O and η=O sites in ^{17}O-enriched $[Nb_6O_{19}]^{8-}$ and $[Ta_6O_{19}]^{8-}$ as a function of pH and temperature.[6,9-11] Three significant differences were observed between the aqueous behavior of the isostructural complexes, suggesting that niobium and tantalum are not as chemically similar as previously thought. First, while protonation (pH decrease) renders both the μ_2-O and η=O sites in $[Nb_6O_{19}]^{8-}$ and $[Ta_6O_{19}]^{8-}$ more labile, the exchange rates of the two oxygen sites in $[Nb_6O_{19}]^{8-}$ become equal at pH values less than 12, but they are never the same in $[Ta_6O_{19}]^{8-}$. Second, the η=O sites exchange slower than the μ_2-O sites in $[Nb_6O_{19}]^{8-}$, but the reverse is true for $[Ta_6O_{19}]^{8-}$. Finally, differences in the activation parameters for $[Nb_6O_{19}]^{8-}$ and $[Ta_6O_{19}]^{8-}$ suggest that the two complexes do not react by the same mechanism.

As part of our interest in further distinguishing the oxide chemistries of niobium and tantalum, we now report differences in solid-state structures of the cluster salts that are consistent with their oxygen-isotope exchange rates. Similar behavior is also observed in the reactivity of Nb- and Ta-bound oxygen atoms at the surfaces of ^{17}O-enriched powders of Nb_2O_5 and Ta_2O_5. In addition, we have developed a new soft chemical route to $[Ta_6O_{19}]^{8-}$ salts. Previously, $[Ta_6O_{19}]^{8-}$ could only be prepared by solid-state alkaline digestion of Ta_2O_5.

Experimental Methods

General Methods and Materials

$Na_7[HNb_6O_{19}]\bullet 15H_2O$ (**1**) was obtained as previously reported and purity was confirmed by infrared spectroscopy and X-ray powder diffraction.[9] $TaCl_5$ (99.8%), $Ta(OC_2H_5)_5$ (99.98%), $Nb(OC_2H_5)_5$ (99.95%), and RbOH (99%, 50 wt.% solution in water) were purchased from Aldrich. NaOH (A.C.S. Grade), NaOH (Certified, 50 wt.% solution in water), KOH (A.C.S. Grade), H_2O_2 (30%), and HNO_3 (A.C.S. Grade Plus), 2-propanol, and Na_3VO_4 (Laboratory Grade) were purchased from Fisher. K_3VO_4 was purchased from Alfa Aesar. Elemental analysis (Na and Ta) was performed by Galbraith Laboratories, Inc. (Knoxville, TN). Thermal analysis was performed with a TA Instruments SDT 2960 for simultaneous thermogravimetric and differential thermal analysis (TGA-DTA) under N_2 flow with a heating rate of 20 °C/min. X-ray powder diffraction was performed with a Bruker D8 Advance diffractometer in Bragg-Brentano geometry with Cu Kα radiation and a diffracted-beam graphite monochromator. Infrared spectra (400-4000 cm^{-1}) were recorded on a Thermo Nicolet 380 FT-IR equipped with a Smart Orbit (Diamond) ATR accessory. All ^{17}O MAS NMR experiments were performed on a Bruker Avance 600 instrument at 81.39 MHz, using a 2.5 mm broadband probe spinning at 30+ kHz. Chemical shifts were referenced to external H_2O, $\delta = 0.0$.

$Rb_3Ta(O_2)_4$ and $K_3Ta(O_2)_4$

The synthesis of $Rb_3Ta(O_2)_4$ and $K_3Ta(O_2)_4$ was slightly modified from the literature method.[12] A 1.75 g (4.9 mmol) sample of $TaCl_5$ was dissolved in 15 mL of 30% H_2O_2 (132 mmol) contained in a 250 mL beaker (within an ice-water bath) with moderate stirring throughout the entire reaction. The temperature of the hydrogen peroxide solution was between 5 – 10 °C before the addition of tantalum(V) chloride. A total of ~4 mL of 50% RbOH (~10 molar) is added in 1-mL aliquots. After 1 – 2 mL of RbOH is added the solution becomes cloudy. However, once the entire 4 mL aliquot of RbOH is added the solution becomes completely clear (but effervescent). Methanol (30 mL) is added to the solution to form a white precipitate, and the mixture is again cooled to 5 – 8 °C. An additional 20 mL of methanol is added, the solution is filtered, washed with two 50-mL aliquots of methanol, and dried in air for 45 min to 1 h. The yield of the product, Rb_3TaO_8, is between 2.40 – 2.60 g (87 – 94% yield). IR (ATR, 1000-400 cm^{-1}): 805.7 (s), 554.8 (m, sh), 522.3 (s), and 422.9 (s). The K-analogue, K_3TaO_8, is prepared by substituting ~13 mL of 4 M KOH. The yield of the product, K_3TaO_8, is 2.07 g (99% yield). IR (ATR, 1000-400 cm^{-1}): 806.8 (s), 551.2 (w, sh), 521.9 (s), and 431.9 (s).

$Na_8[Ta_6O_{19}]\bullet 15H_2O$, 2

A 5 g (8.8 mmol) sample of $Rb_3Ta(O_2)_4$ was dissolved in 50 mL of 0.2 M RbOH at 80 – 90 °C with moderate stirring, and 0.007 g of Na_3VO_4 (0.038 mmol) was added to the solution, upon which it became yellow and effervescent. Once the solution was colorless (15 – 30 min), the temperature was increased to 100 °C and the volume reduced to 10 – 15 mL. The solution was cooled to room temperature, filtered with a 0.45 μm syringe, and placed in a refrigerator. Colorless, diffraction quality crystals of $Rb_6Na_2[Ta_6O_{19}]\bullet 21H_2O$‡ form over 1–2 days (yield 3.2 g, 91% based on Ta). A 3.2 g sample of $Rb_6Na_2[Ta_6O_{19}]\bullet 23H_2O$ was dissolved in 78 mL of water, and this solution was added dropwise to 310 mL of 0.31 M NaOH, heated to 90 °C. The solution was cooled to room temperature, and a white crystalline material formed within several minutes. After 3 days evaporation in air, the solution was filtered to yield a mixture of colorless

needles and hexagons,[§] where the colorless needles are the desired phase. The mixture was redissolved in 285 mL of water (heated to 60 °C), and 50 wt. % NaOH was added dropwise until only the colorless needles start to recrystallize. A total of 2.40 g of product was collected (96% yield based on Ta). Larger needles, more suitable for X-ray diffraction studies, were prepared by slow evaporation of a solution 0.2 mM in $Rb_6Na_2[Ta_6O_{19}]\bullet 23H_2O$ and 2 M NaOH. IR (ATR, 1000–400 cm^{-1}): 833.0 (s), 647.3 (s), and 520.7 (s). Anal. Calcd for $Na_8[Ta_6O_{19}]\bullet 15H_2O$: Na, 9.97%; ($H_2O$), 14.6%; Ta, 58.9%. Found: Na, 9.68%; (H_2O), 14.4%; Ta, 59.1%.

^{17}O Enriched $K_7Na[Ta_6O_{19}]\bullet 14H_2O$, 3

A 4.00 g (9.4 mmol) sample of $K_3Ta(O_2)_4$, 3.83 g (68 mmol) of KOH, and 0.137 g (0.6 mmol) of K_3VO_4 were added to 10 mL of water (20% ^{17}O) and the mixture was refluxed and stirred until a clear solution was obtained (~30–45 min). The warm solution was filtered with a 0.45 μm syringe, and 2.76 g of crystalline material was obtained by slow evaporation of the solution at room temperature over 2 days (91% yield based on Ta).

Crystallographic Studies of 1 and 2

Single-crystal X-ray diffraction of **1** and **2** was performed on a Bruker AXS SMART-APEX CCD diffractometer with graphite monochromated Mo Kα (0.71073 Å) radiation. Data collection and reduction were carried out with SMART 5.054 (Bruker, 1998) and SAINT 6.02 (Bruker, 2001) software, respectively. An empirical absorption correction was applied

Table 1. Summary of Crystallographic Data and Structure Refinement for **1** and **2**.

Complex	1	2
Empirical Formula	$H_{31}O_{34}Na_7Nb_6$	$H_{30}O_{34}Na_8Ta_6$
Formula Weight	1293.59	1843.82
Space Group	*P*mnn (no. 58)	*P*mnn (no. 58)
Unit Cell *a*/Å	10.0632(5)	10.0215(16)
b/Å	12.1301(7)	12.007(2)
c/Å	12.6705(7)	12.761(2)
V/Å^3	1546.66(15)	1535.5(4)
Z	2	2
T	173 K	173 K
d (calc)/g cm^{-3}	2.778	3.988
λ/Å	0.71073	0.71073
μ/cm^{-1}	2.369	21.524
2θ min/° max/°	4.64 50.52	4.66 56.04
final R_1[a] [I > 2σ(I)]	0.0165	0.0189
final wR_2[b] [I > 2σ(I)]	0.0479	0.0499
GOF	1.217	1.142

[a] $R_1 = \Sigma||F_o| - |F_c||/|F_o|$.
[b] $wR_2 = \{\Sigma[w(F_o^2 - F_c^2)^2] / \Sigma[w(F_o^2)^2]\}^{0.5}$.

using SADABS v. 2.03 (Sheldrick, G. *SADABS*; University of Göttingen: Göttingen, Germany, 1999). All subsequent structure solution and refinement were performed within the WinGX

system. The structure was solved by Direct Methods (program SIR97) and refined by full matrix least-squares on F^2 (SHELX97). The non-standard space group setting P*mnn* (no. 48) was chosen to be consistent with the original structure reported by Goiffon in 1980.[13] Bond valence sum (BVS) calculations were used to help assign the protonation state of oxygen atoms.[14] Crystallographic data are summarized in Table 1 and additional details may be obtained from the Fachinformationszentrum Karlsruhe, 76344 Eggenstein-Leopoldshafen, Germany, on quoting registry numbers CSD-417857 and CSD-417856 for complex **1** and **2**, respectively.

Hydrous $^{17}O_5Nb_2$ and $^{17}O_5Ta_2$

A 3.36 g (10.6 mmol) sample of $Nb(OC_2H_5)_5$ or 4.29 g of $Ta(OC_2H_5)_5$ was added to 30 mL of 2-propanol with stirring and 1 mL of 0.1 M HNO_3 was subsequently added to obtain a white to yellow precipitate. After 30 min., the precipitate was collected by filtration and dried under vacuum at 60 °C for 16 h. The powder was suspended in 2 mL of water (20% ^{17}O) in a 20 mL capped vial and heated to 40 °C for 2 h. The resulting solid was filtered and dried under vacuum at 60 °C for 16 h. After acquiring an ^{17}O MAS NMR spectrum on hydrous $^{17}O_5Ta_2$, it was annealed at 800 ˚C in air for 2 h, and an ^{17}O MAS NMR spectrum was again collected.

Hydrothermal Reactions

A 0.22 mmol sample of **2**, **3**, or $Na_8[Ta_5NbO_{19}]$ was dissolved in 8 mL of 0.1-1.0 M NaOH or 0.1-0.75 M KOH contained in a 23 mL Teflon liner for a Parr reactor. The solution was placed in an oven at 200 °C for 16 h. After the sample was cooled to room temperature, a microcrystalline powder was collected by vacuum filtration, washed with ethanol, and dried in air.

Results and Discussion

Synthesis

The synthesis of alkali salts of $[Nb_6O_{19}]^{8-}$ (or $[H_xNb_6O_{19}]^{(8-x)-}$) and $[Ta_6O_{19}]^{8-}$ by solid-state alkaline digestion of Nb_2O_5 and Ta_2O_5, respectively, is well known.[4-6,15,16] Previously, we reported that alkali salts of $[Nb_6O_{19}]^{8-}$ could also be prepared by the dissolution of hydrous Nb_2O_5 into alkali hydroxide solutions.[9,17] However, the limited commercial availability of hydrous Ta_2O_5, as well as the much poorer solubility of laboratory-produced hydrous Ta_2O_5, prompted us to consider alternative routes to $[Ta_6O_{19}]^{8-}$. The aqueous chemistry of niobium and tantalum is somewhat restrictive, but peroxide complexes of these metals have attracted considerable attention as soluble precursors for the soft chemical preparation of a range of oxide materials.[12] We have found that alkali salts of $[Ta_6O_{19}]^{8-}$ may be prepared by the prolonged boiling of $[Ta(O_2)_4]^{3-}$ in conditions alkaline enough to arrest formation of tantalum oxide. Boiling times can be significantly decreased by $[VO_4]^{3-}$-catalyzed decomposition of the peroxide ligands. Crystallization of the material is accomplished by slow evaporation of the solution at room temperature. This new peroxide-decomposition method greatly facilitated the preparation of ^{17}O-enriched product because high yields of analytically pure compound could be obtained from a single crystallization.

Alkali salts of $[Nb_6O_{19}]^{8-}$ may also be synthesized from $[Nb(O_2)_4]^{3-}$. We attempted to prepare a family of mixed niobium-tantalum Lindqvist clusters by varying the ratio of $[Nb(O_2)_4]^{3-}$ to $[Ta(O_2)_4]^{3-}$. Although the composition put into the synthesis is generally reflected in the product (Table 2), according to the refinement of single-crystal data on a series of

compounds formulated as $K_7Na[Ta_{6-x}Nb_xO_{19}]\bullet 14H_2O$ (x = 1-6), ^{17}O NMR data suggest the product is actually a mixture of $[Nb_6O_{19}]^{8-}$, $[Ta_6O_{19}]^{8-}$, and $[Ta_{6-x}Nb_xO_{19}]^{8-}$. While these mixed phases are not particularly interesting from a cluster perspective, they do provide more evidence for the differences between Ta and Nb structural and reactivity chemistry (see below), and also may serve as atomically mixed precursors for mixed metal-oxide materials.

Table 2. Compositional Data for Mixed Group VA Clusters

Synthesis Composition	$TaNb_5$	Ta_2Nb_4	Ta_3Nb_3	Ta_4Nb_2
Site 1 (% Ta)	25	41	57	73
Site 2 (% Ta)	16	27	44	60
Site 3 (% Ta)	19	31	49	66
Site 4 (% Ta)	17	28	46	62
Site 5 (% Ta)	17	28	47	63
Site 6 (% Ta)	17	28	45	62
Refinement Composition	$Ta_{1.1}Nb_{4.9}$	$Ta_{1.8}Nb_{4.2}$	$Ta_{2.9}Nb_{3.1}$	$Ta_{3.9}Nb_{2.1}$

Structural Studies

A global average of bond lengths and angles from reported structures of $[Nb_6O_{19}]^{8-}$ and $[Ta_6O_{19}]^{8-}$ reveals that the two anions are difficult to distinguish, as expected from the lanthanide contraction.[4,5,15-18] Key structural differences in the clusters are also obscured by the high surface charge of the ions (0.32 charge/atom), which gives rise to strong crystal packing interactions. To elucidate any differences, Table 3 compares isostructural salts of $[Nb_6O_{19}]^{8-}$ and $[Ta_6O_{19}]^{8-}$. The results indicate a pronounced increase in M(η=O) bond lengths and M-μ_2-O-M angles in $[Ta_6O_{19}]^{8-}$, although the central μ_6-O-M bond lengths are identical within experimental error. There is also a slight decrease in μ_2-O-M bond lengths in $[Ta_6O_{19}]^{8-}$. Differences in the

Table 3. Structural Parameters for Group VA Lindqvist Ions.

Compound(s)	M=O_t (Å)[a]	μ_6-O-M (Å)[a]	μ_2-O-M (Å)[a]	M-μ_2-O-M(°)[b]
All $[H_xNb_6O_{19}]^{(8-x)-}$	1.793	2.366	1.990[c]	114.3
All $[Ta_6O_{19}]^{8-}$	1.802	2.360	1.982	114.7
$Na_7[HNb_6O_{19}]\bullet 15H_2O$	1.770	2.379	1.994	114.5
$Na_8[Ta_6O_{19}]\bullet 15H_2O$	1.799	2.380	1.992	115.0
$K_7Na[Nb_6O_{19}]\bullet 14H_2O$	1.796	2.364	1.993	114.0
$K_7Na[Ta_6O_{19}]\bullet 14H_2O$	1.813	2.365	1.986	114.6
$Rb_8[Nb_6O_{19}]\bullet 14H_2O$	1.804	2.355	1.985	114.0
$Rb_8[Ta_6O_{19}]\bullet 14H_2O$	1.817	2.358	1.979	114.7
$Cs_8[Nb_6O_{19}]\bullet 14H_2O$	1.804	2.360	1.987	114.2
$Cs_8[Ta_6O_{19}]\bullet 14H_2O$	1.811	2.353	1.975	115.2

[a]Error ±0.003 Å. [b]Error ±0.1°. [c]Excludes μ_2-OH-M bonds.

structural parameters summarized in Table 3, along with recent kinetics studies, suggest that $[Nb_6O_{19}]^{8-}$ has a more basic bridging μ_2-O site and $[Ta_6O_{19}]^{8-}$ has a more basic η=O site.

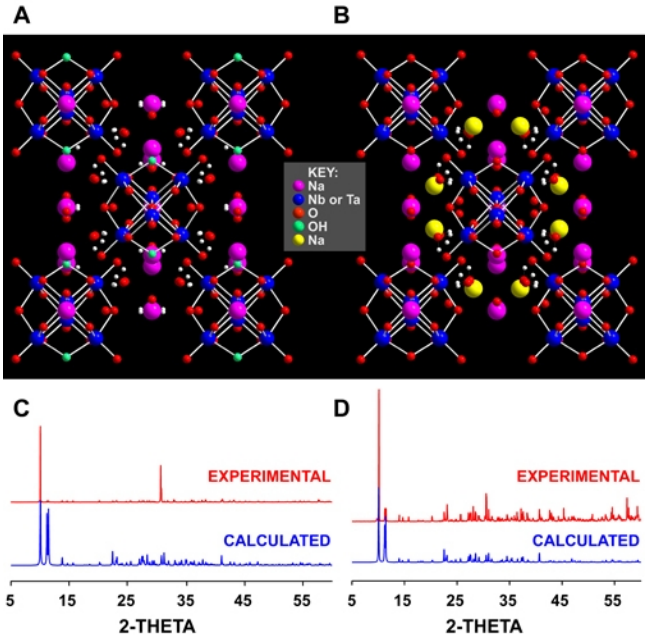

Figure 1. Difference in charge-balancing of isostructural $Na_7[HNb_6O_{19}]\bullet 15H_2O$ (**1**) and $Na_8[Ta_6O_{19}]\bullet 15H_2O$ (**2**) is illustrated in A and B, respectively. In **1**, the green spheres are half-occupied m_2-OH sites, giving one proton per $[HNb_6O_{19}]^{7-}$ cluster. In **2**, the yellow spheres are 25% occupied sodium sites, giving an extra one sodium per $[Ta_6O_{19}]^{8-}$ cluster. C and D show the X-ray powder diffraction spectra of **1** and **2**, respectively, with the calculated pattern in blue and the experimental pattern in red. Differences in peak intensity between the experimental and calculated patterns are due to strong preferred orientation resulting from the acicular crystal morphology of **1** and **2**.

In the mixed $[Ta_{6-x}Nb_xO_{19}]^{8-}$ salts (Table 2), of the six MO_6 positions of the cluster (all M sites are crystallographically unique in this monoclinic phase), site 1 and site 3 show the highest preference for Ta over Nb. In these $[M_6O_{19}]^{8-}$ clusters that are quite distorted by lattice packing effects, site 1 and site 3 exhibit the longest terminal oxygen bond lengths. While these distortions are predominantly a result of packing effects, as indicated by the distortions also observed in the end-members ($[Nb_6O_{19}]^{8-}$ and $[Ta_6O_{19}]^{8-}$),[15] Ta clearly favors this geometry with more basic η=Ọsites.

More evidence for differences in oxygen ligand basicity is revealed in the solution behavior of the clusters. Stepwise proton uptake occurs at the μ_2-O sites of $[Nb_6O_{19}]^{8-}$ in solution from pH 14 to 9.[9,10] Under similar conditions, a protonated $[Ta_6O_{19}]^{8-}$ has never been observed in solution, which is consistent with decreased μ_2-O-Ta basicity.[19]

Several solid-state structures of $[H_2Nb_6O_{19}]^{6-}$ alkali salts and one $[HNb_6O_{19}]^{7-}$ (potassium salt) have been reported and in each case the proton(s) resides on a bridging oxygen(s), μ_2-OH.[4,13,17,20] Corresponding to solution protonation studies, no solid-state salts of $[H_2Ta_6O_{19}]^{6-}$ or $[HTa_6O_{19}]^{7-}$ have ever been isolated.[5,15,16] The first structure reported for a $[H_xNb_6O_{19}]^{(8-x)-}$ ($0 \leq x \leq 3$) salt was by Lindqvist and refined by Goiffon 27 years later, formulated as $Na_7(H_3O)[Nb_6O_{19}]\bullet 14H_2O$.[4,13] The isostructural powder pattern for a sodium tantalate described as $Na_{14}Ta_{12}O_{37}\bullet 31H_2O$ is also deposited in the JCPDF database.[21] However, new single crystal X-ray analyses of these salts along with supporting compositional and ^{23}Na MAS NMR studies strongly suggest they are actually $Na_7[HNb_6O_{19}]\bullet 15H_2O$ (**1**) and $Na_8[Ta_6O_{19}]\bullet 15H_2O$ (**2**). These salts are particularly indicative of the differences in Ta-oxo and Nb-oxo chemistry, in that the salts are isostructural, but the Nb cluster is protonated and the Ta cluster is not protonated in isostructural lattices. In these phases, seven sodium atoms and all fifteen water molecules are located in identical unit cell positions (Figure 1). However, the eighth charge-balancing sodium of the $[Ta_6O_{19}]^{8-}$ salt (shaded yellow in Figure 1B) is located in close proximity to a bridging oxygen (Na-O_b, 2.55 Å), whereas this same bridging oxygen site (shaded green in Figure 1A) is protonated in the $[HNb_6O_{19}]^{7-}$ salt. The location of the proton for **1** on a cluster bridging site, μ_2-OH, was first proposed from the infrared spectrum and ^1H MAS NMR.[9] Furthermore, the $(H_3O)^+$ initially proposed by Goiffon seemed improbable, given the alkaline conditions for the

synthesis of **1**.[13] Additional evidence for the isostructural nature of **1** and **2** is provided by the X-ray powder diffraction spectra of the bulk samples (Figure 1 C and D).

The central oxygen of the Lindqvist cluster sits on (0.5,0.5,0) and therefore the clusters have crystallographically imposed 2/m symmetry. The μ_2-OH of **1** is disordered over the two O7 sites per cluster, so it could not be located directly from the electron density map. However, the bond length of the "half-protonated" Nb1-O7 (2.067 Å) is between that of a nonprotonated Nb-μ_2-O bond length (2.0 Å) and that of a fully protonated Nb-μ_2-OH bond length (2.2 Å). Additionally, the BVS of O7 is only 1.484, and a half-occupied proton would bring this value up to 2.084. The structure of **2** was refined with a slightly smaller unit cell than **1** (1535.5 Å^3 vs. 1546.7 Å^3), initially using the atomic positions of **1**. The Ta1-O7 bond length is 1.987 Å; with a BVS of 1.942, suggesting no protonation at this site. Furthermore, a significant peak remained in the electron density map of **2**, which was refined as a partially occupied sodium site, Na5. The occupancy was fixed at 0.25 to accommodate charge-balancing requirements and thermal parameters, and to avoid other disordered Na5 sites that are in close proximity, as well as partially occupied water sites, O14 and O15. Further disorder is imparted on the structure of **2** at the O14 water site. In **1**, O14 sits on a special position. In **2**, O14 moves 0.45 Å to a general position, resulting in two half occupied O14 sites, 0.9 Å away from each other. The overall increased sodium/water disorder in **2** gives rise to a ^{23}Na MAS NMR spectrum with broader and less well-defined peaks than that of **1**; further supporting the differences between the two structures.

^{17}O-NMR studies of hydrous Nb_2O_5 and Ta_2O_5

The differences in the reactivity of Nb(V)- and Ta(V)-bound oxygens are also manifested at the surfaces of ^{17}O-enriched powders of Nb_2O_5 and Ta_2O_5; the exchange of terminal and bridging oxygens proceed at different rates. Amorphous oxides of Nb(V) and Ta(V) were formed from room-temperature hydrolysis and condensation reactions of the respective alkoxides and the surfaces were enriched by mild treatment with $H_2{}^{17}O$ at 40 ˚C to obtain sufficient labeling, predominantly at the surface and not the bulk. The ^{17}O MAS NMR spectra of the oxides are shown in Figure 2. In the hydrous Nb_2O_5 spectrum, three major resonances are

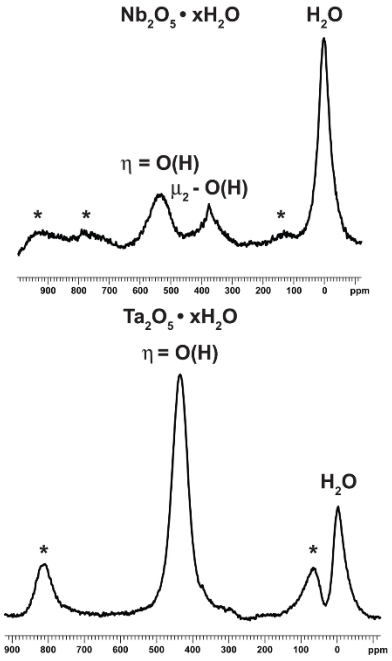

Figure 2. ^{17}O MAS NMR spectra of ^{17}O-surface enriched hydrous Nb_2O_5 (top) and Ta_2O_5 (bottom) under mild conditions. Like the model clusters, the surface of Ta_2O_5 exhibits slower exchange of its μ_2-O oxygen sites, in that insufficient exchange at this site results in no ^{17}O signal. * denotes spinning side bands.

observed: the H_2O resonance at δ = +1 ppm (57%), the μ_2-O(H) resonance at δ = +373 ppm (15%), and the η=OH resonance at δ = +535 ppm (28%). The resonances of the different oxygen types at the Nb_2O_5 surface match well with those of the corresponding $[Nb_6O_{19}]^{8-}$ cluster (386 and 594 ppm respectively).[9,10] The hydrous Ta_2O_5 spectrum has a major resonance at δ = +437 ppm (81%) and an H_2O peak at -3 ppm (19%). The oxide resonance lies between that of a μ_2-O resonance (329 ppm) and a η=O (473 ppm) resonance of the Lindqvist ion; and could not be unambiguously assigned initially, although it is closer to the terminal η=O resonance. Annealing the sample at 800 ˚C resulted in two peaks, δ = +473 (41%) and +331 (29%) ppm, corresponding exactly with the terminal η=O and bridging μ_2-O respectively of the $[Ta_6O_{19}]^{8-}$ Lindqvist ion (Figure 3). A third sharp peak at 66 ppm (30%) was assigned to oxygen atoms that have diffused below the surface into the more ordered framework of the annealed Ta_2O_5. Annealing the Ta_2O_5 sample resulted in cross-linking and bridging via dehydration to obtain the enriched μ_2-O oxygen sites. The results suggest that the oxygen exchange at the surface takes place readily at both terminal and bridging oxygen sites for Nb_2O_5, but only at terminal sites for Ta_2O_5, consistent with the higher reactivity of the terminal oxygens in the $[Ta_6O_{19}]^{8-}$ cluster.

These studies provide additional evidence that the Lindqvist ions are excellent structural and reactivity models for the corresponding metal oxide surfaces at aqueous interfaces. The surface oxygens of these poorly ordered oxides (amorphous by powder X-ray diffraction) appear identical to the bridging and terminal oxygen sites of the Lindqvist clusters by ^{17}O MAS NMR. Furthermore, the exchange rates between surface oxygens and bulk water are analogous to the exchange behavior of the model clusters.

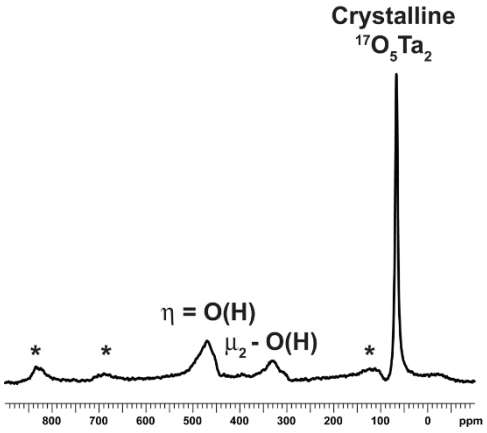

Figure 3. ^{17}O MAS NMR spectrum of hydrous $^{17}O_5Ta_2$ annealed at 800 ˚C. Spinning sidebands are denoted with *.

Hydrothermal Reactions

In order to assess the value of $[Ta_6O_{19}]^{8-}$ and $[Ta_{6-x}Nb_xO_{19}]^{8-}$ (x =1-6) as soluble precursors for the hydrothermal synthesis of commercially viable pyrochlore and perovskite phases, **2**, **3**, and $Na_8[Ta_5NbO_{19}]$ were heated to 200 °C for 16 h in aqueous NaOH or KOH, and the resulting powders were characterized by X-ray powder diffraction. The results are summarized in Figure 4. At low concentrations of NaOH (0.1 to 0.25 M), **2** is cleanly converted to the pyrochlore $Na_2Ta_2O_6$ (Figure 4A and 4B). However, at higher temperatures (Figure 4C) and higher NaOH concentration (Figure 4D and 4E), a mixture of $Na_2Ta_2O_6$ and the perovskite $NaTaO_3$ are obtained. The potassium analogue, $K_2Ta_2O_6$, can also be obtained by reacting **3** in 0.1 to 0.75 M KOH (Figure 4F and 4G). Finally, $Na_8[Ta_5NbO_{19}]$ was heated to 200 °C in 0.1 M NaOH with the goal of obtaining $Na_2Ta_{1.67}Nb_{0.33}O_6$, but the X-ray powder pattern (Figure 4H) suggests that a mixture of $Na_2Ta_2O_6$ and $NaNbO_3$ were obtained instead.

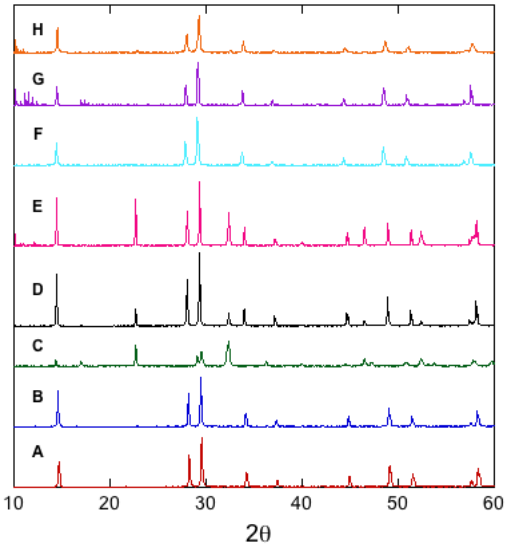

Figure 4. X-ray powder patterns of phases prepared by heating **2**, **3**, or $Na_8[Ta_5NbO_{19}]$ to 200 °C for 16 h in aqueous NaOH or KOH. **(A) 2** in 0.1 M NaOH **(B) 2** in 0.25 M NaOH **(C) 2** in 0.25 M NaOH heated to 900 °C by TGA at a rate of 20 °C/min **(D) 2** in 0.5 M NaOH **(E) 2** in 1 M NaOH **(F) 3** in 0.1 M KOH **(G) 3** in 0.75 M KOH **(H)** $Na_8[Ta_5NbO_{19}]$ in 0.1 M NaOH.

Conclusions

The results presented here indicate there are significant differences in niobium and tantalum oxide structures and reactivity in both model clusters and interfaces. The key difference seems to lie in the protonation chemistry, where stable μ_2-OH sites are favored in niobium oxide materials and transient, unstable η=OH sites form in tantalum oxide materials. Since protonation is a key step in oxide dissolution, the inability to form stable, protonated, soluble tantalate species is perhaps one reason that all aspects of polyoxotantalate chemistry are more underdeveloped than polyoxoniobate chemistry, illustrated by the variety of cluster geometries and transition metal-$[Nb_6O_{19}]^{8-}$ complexes that have been characterized in the solid-state, many in the last five years.[22-32] Non-protonated $[Ta_6O_{19}]^{8-}$ as an alkali salt and as a complex with rhenium are the only polyoxotantalates that have been crystallized.[5,15,16,24]

Finally, while discrete clusters are frequently used as structural models for interfaces, they rarely serve as reactivity models.[8,33] The results presented here suggest there is much yet to be learned in our continued work regarding the behavior of mixed metal-oxo clusters, including those substituted with tungsten or molybdenum to obtain more acidic oxygen sites.

Notes and References

‡ The molecular formula of this intermediate was determined by single-crystal X-ray diffraction. Space group: R -3, a = 12.347(3) Å, c = 46.554(1) Å, V = 6147(2) Å^3. Additional details can be obtained from the Fachinformationszentrum Karlsruhe, 76344 Eggenstein-Leopoldshafen, Germany, on quoting registry number CSD-418081.

§ We were only able to obtain a unit cell for this hexagonal phase due to the lamellar and highly twinned nature of the crystals: hexagonal, -3, a = 12.404(2) Å, c = 31.504(5) Å, V = 4198(2) Å^3. The infrared spectrum of the mixture of crystals suggests this is another $[Ta_6O_{19}]^{8-}$ salt.

1. N. N. Greenwood and A. Earnshaw, in *Chemistry of the Elements*, Pergamon Press, 1984.
2. N. Ramadass, *Mater. Sci. Eng.* , 1978, **36**, 231.
3. M. A. Subramanian, G. Aravamudan, and G. V. Subba Rao, *Prog. Solid State Chem.*, 1983, **15**, 55.
4. I. Lindqvist, *Ark. Kemi*, 1953, **5**, 247.
5. I. Lindqvist and B. Aronsson, *Ark. Kemi*, 1953, **7**, 49.
6. M. Filowitz, R. K. C. Ho, W. G. Klemperer, and W. Shum, *Inorg. Chem.*, 1979, **18**, 93.
7. M. T. Pope, in *Heteropoly and Isopoly Oxometalates*, Springer-Verlag, 1983.
8. V. W. Day and W. G. Klemperer, *Science*, 1985, **228**, 533.

9. T. M. Alam, M. Nyman, B. R. Cherry, J. M. Segall, and L. E. Lybarger, *J. Am. Chem. Soc.*, 2004, **126**, 5610.
10. J. R. Black, M. Nyman, and W. H. Casey, *J. Am. Chem. Soc.*, 2006, **128**, 14712.
11. E. M. Balogh, T. M. Anderson, J. R. Rustad, M. Nyman, and W. H. Casey, *Inorg. Chem.*, 2007, **46**, 7032.
12. D. Bayot and M. Devillers, *Coord. Chem. Rev.*, 2006, **250**, 2610.
13. A. Goiffon, E. Philippot, and M. Maurin, *Rev. Chim. Miner.*, 1980, **17**, 466.
14. I. D. Brown and D. Altermatt, *Acta Cryst.*, 1985, **B41**, 244.
15. F. Pickhard and H. Hartl, *Z. Anorg. Allg. Chem.*, 1997, **623**, 1311.
16. H. Hartl, F. Pickhard, F. Emmerling, and C. Röhr, *Z. Anorg. Allg. Chem.*, 2001, **627**, 2630.
17. M. Nyman, T. M. Alam, F. Bonhomme, M. A. Rodriguez, C. S. Frazer, and M. E. Welk, *J. Cluster Sci.*, 2006, **17**, 197.
18. T. M. Anderson, S. G. Thoma, F. Bonhomme, M. A. Rodriguez, H. Park, J. B. Parise, T. M. Alam, J. P. Larentzos, and M. Nyman, *Cryst. Growth Des.*, 2007, **7**, 719.
19. W. H. Nelson and R. S. Tobias, *Inorg. Chem.*, 1963, **2**, 985.
20. T. Ozeki, T. Yamase, H. Naruke, and Y. Sasaki, *Bull. Chem. Soc. Jpn.*, 1994, **67**, 3249.
21. M. Muller, *Rev. Chim. Miner.*, 1970, **7**, 359.
22. C. M. Flynn Jr. and G. D. Stucky, *Inorg. Chem.*, 1969, **8**, 332.
23. E. J. Graeber and B. Morosin, *Acta Crystallgr.*, 1977, **B33**, 2137.
24. A. V. Besserguenev, M. H. Dickman, and M. T. Pope, *Inorg. Chem.*, 2001, **40**, 2582.
25. K. Hegetschweiler, R. C. Finn, R. S. Rarig Jr., J. Sander, S. Steinhauser, M. Worle, and J. Zubieta, *Inorg. Chim. Acta*, 2002, **337**, 39.
26. M. Nyman, F. Bonhomme, T. M. Alam, M. A. Rodriguez, B. R. Cherry, J. L. Krumhansl, T. M. Nenoff, and A. M. Sattler, *Science*, 2002, **297**, 996.
27. M. Nyman, F. Bonhomme, T. M. Alam, J. B. Parise, and G. M. B. Vaughan, *Angew. Chem. Int. Ed.*, 2004, **43**, 2787.
28. M. Nyman, A. J. Celestian, J. B. Parise, G. P. Holland, and T. M. Alam, *Inorg. Chem.*, 2006, **45**, 1043.
29. R. P. Bontchev and M. Nyman, *Angew. Chem. Int. Ed.*, 2006, **45**, 6670.
30. M. Maekawa, Y. Ozawa, and A. Yagasaki, *Inorg. Chem.*, 2006, **45**, 9608.
31. D. Laurencin, R. Thouvenot, K. Boubekeur, and A. Proust, *Dalton Trans.*, 2007, 1334.
32. R. P. Bontchev, E. L. Venturini, and M. Nyman, *Inorg. Chem.*, 2007, **46**, 4483.
33. M. I. Khan, E. Yohannes, and D. Powell, *Inorg. Chem.*, 1999, **38**, 212.

Distribution

2	MS9018	Central Technical Files	8944
2	MS0899	Technical Library	4536
1	MS0123	D. Chavez, LDRD Office	1011
1	MS0754	M. J. Rigali	6316
1	MS0754	M. Nyman	6316
1	MS0754	T. M. Anderson	6316
1	MS0735	John A. Merson	6310